Dear editor,

Thank you for handling our paper. We are grateful that the two referees are helpful to improve our work. We provide a point-by-point response to the reviews and revised the manuscript accordingly.

We are now improving our algorithm to process wind fields to accurately estimate the CO_2 flux and are also extending our work to a global scale. To be consistent with our ongoing work, we have decided to reprocess all of the results of this study using our current codes. The conclusion and discussion are not changed, while the emission estimation results for China's cities are slightly different from the previous version. We have updated the manuscript with all of the new values and new figures. The marked-up manuscript version shows what we have revised.

Thank you for your consideration of this manuscript.

Sincerely,
Bo Zheng on behalf of all co-authors

Referee #1:

General comments.

The manuscript reports good progress in quantifying multiple megacity emissions of CO_2 in China using a plume transport model and CO_2 observations by OCO-2 satellite. The mean estimate of the emissions from selected megacity areas is comparable with inventory data. The manuscript is well written and can be recommended for publication after minor revisions, taking into the account the following comments:

Response:

We thank the referee for the positive comments on our manuscript.

Detailed comments.

Line 42 As for instrument noise (not retrieval noise) it may be better to use a number in the order of 0.3 - 0.6 ppm as in (Worden et al., 2017)

Response:

This sentence has been rewritten as "an instrument noise typically around 0.3–0.6 ppm (Worden et al., 2017)".

Line 49 Authors write "To our knowledge, no attempt has been made yet to infer anthropogenic emissions from actual satellite data over a large area or a long period to evaluate a large-scale CO_2 budget." Suggest being more specific here and write as "actual OCO-2 data", otherwise, when speaking about satellites, there is a study by Janardanan et al., (2016) using several years of CO_2 data for assessing emissions from large regions. Also adding somewhere reference to Kort et al., 2012 is useful from historical context.

Response:

We now use the expression "actual OCO-2 data" and have added the reference to Kort et al. (2012).

Line 176 "The ceiling height of 500 m is comparable to the maximum height that smoke plumes from power plants and industrial plants typically reach." The assumption seems to be weak, as turbulent mixing is supposed to mix CO_2 up to PBL top, exceeding 500 m in many occasions. The practical choice of using a mean wind vector below 500 m may be driven by other reasons.

Response:

To quantify cross-sectional CO_2 fluxes, we need to know the horizontal wind direction and wind speed at the CO_2 plume height (Nassar et al., 2017). For a power plant, Nassar et al. (2017) used the wind vector at the stack height. Since this study focuses on cities that have emission sources with various stack heights, we used the average wind below 500 m following Beirle et al. (2011).

Line 222 More informative reference to ODIAC is given by Oda et al., (2018)

Response:

We have added the reference to Oda et al. (2018) in the revised manuscript.

Line 267 For CO2-M there is a recent mission paper by Janssens-Maenhout et al. (2020)

Response:

We have added the reference to Janssens-Maenhout et al. (2020).

Line 210 Summertime uptake by green spaces in a city should not be used as an explanation here as vegetation uptake is also present in the background used as reference for estimating enhancements.

Response:

The XCO_2 enhancement tends to be lower in summer than in winter (Mitchell et al., 2018) due to the photosynthetic uptake by plants. This phenomenon makes $FFCO_2$ signal not easily separated from the surrounding background, which could partly explain the slight underestimates in the $FFCO_2$ fluxes from OCO-2 XCO_2 retrievals in summer. We have clarified it in the manuscript.

Line 235 There is an impression that there is a 200-300% disagreement between MEIC and other inventories in cities, and it is caused by misplacing industrial emissions. There are other factors apart from placing industrial emissions. ODIAC is using a simple disaggregation of emissions by using nightlights, which may lead to underestimation of road emissions, as found by Gateley and Hutyra (2017), so it is supposed to be missing some emissions in cites still it was found by Gateley and Hutyra (2017) to correlate well with the detailed inventory at 5 km resolution. EDGAR inventory is not supposed to suffer from misplacing industrial emissions to the same extent as ODIAC thus there should be another reason for disagreement. A reader would benefit from providing more details on scale and reason for discrepancies between the inventories in the target areas.

Response:

We provide a brief discussion on the discrepancies between MEIC and other inventories as follows.

"The large discrepancies are not surprising since global emission inventories typically involve large uncertainties at city scales (Gately and Hutyra, 2017; Gurney et al., 2019), because they disaggregate national emissions to gridded maps with simple proxies like population or nighttime light in the countries like China where they lack detailed direct local information. Only large power plants have exact geographic locations (from the CARMA global database (Wheeler and Ummel, 2008)), in principle, not all of the industrial plants like MEIC. The ODIAC uses nightlights to disaggregate national emission estimates to grid cells, which may lead to an underestimation of road emissions in cities (Gately and Hutyra, 2017) and a misplacing of industrial emissions. The EDGAR relies on point source locations to allocate emissions in space while it still suffers from missing local information in China, and gridded population maps have to be used instead. Such an emission mapping approach overestimates emissions over densely populated cities in China (Zheng et al., 2017), because the industry plants, the primary CO_2 emission sources in China, are located far away from densely urban areas. The MEIC inventory estimates industrial emissions at the facility scale, transport emissions at the county scale, and residential emissions at the provincial scale, which can achieve better spatial accuracy in emissions estimates than the global emission inventories."

References

Beirle, S., Boersma, K. F., Platt, U., Lawrence, M. G., and Wagner, T.: Megacity Emissions and Lifetimes of Nitrogen Oxides Probed from Space, Science, 333, 1737-1739, doi: 10.1126/science.1207824, 2011.

Mitchell, L. E., Lin, J. C., Bowling, D. R., Pataki, D. E., Strong, C., Schauer, A. J., Bares, R., Bush, S. E., Stephens, B. B., Mendoza, D., Mallia, D., Holland, L., Gurney, K. R., and Ehleringer, J. R.: Long-term urban carbon dioxide observations reveal spatial and temporal dynamics related to urban characteristics and growth, Proc. Natl. Acad. Sci., 115, 2912-2917, doi: 10.1073/pnas.1702393115, 2018.

Nassar, R., Hill, T. G., McLinden, C. A., Wunch, D., Jones, D. B. A., and Crisp, D.: Quantifying CO_2 Emissions From Individual Power Plants From Space, Geophys. Res. Lett., 44, 10,045-010,053, doi: 10.1002/2017gl074702, 2017.

References

Janardanan, R., Maksyutov, S., Oda, T., Saito, M., Kaiser, J. W., Ganshin, A., Stohl, A., Matsunaga, T., Yoshida, Y., and Yokota, T.: Comparing GOSAT observations of localized CO_2 enhancements by large emitters with inventory-based estimates, Geophys. Res. Lett., 43, 3486-3493, doi:10.1002/2016GL067843, 2016.

Janssens-Maenhout, G., B. Pinty, M. Dowell, H. Zunker, E. Andersson, et al: Towards an operational anthropogenic CO2 emissions monitoring and verification support capacity. Bull. Amer. Meteor. Soc., https://doi.org/10.1175/BAMS-D-19-0017.1, 2020.

Kort, E. A., Frankenberg, C., Miller, C. E., and Oda, T.: Space-based observations of megacity carbon dioxide, Geophys. Res. Lett., 39, L17806, doi:10.1029/2012GL052738., 2012.

Oda, T., Maksyutov, S., and Andres, R. J.: The Open-source Data Inventory for Anthropogenic CO_2, version 2016 (ODIAC2016): a global monthly fossil fuel CO_2 gridded emissions data product for tracer transport simulations and surface flux inversions, Earth Syst. Sci. Data, 10, 87–107, https://doi.org/10.5194/essd-10-87-2018, 2018.

Worden, J. R., Doran, G., Kulawik, S., Eldering, A., Crisp, D., Frankenberg, C., O'Dell, C., and Bowman, K.: Evaluation and attribution of OCO-2 XCO_2 uncertainties, Atmos. Meas. Tech., 10, 2759–2771, https://doi.org/10.5194/amt-10-2759-2017, 2017.

Referee #2:

The study by Zheng et al. uses the complete XCO_2 data record available from the OCO-2 satellite instrument to estimate the CO_2 emissions of 60 individual sources (cities, power plants, industrial areas) in China, accounting for almost one fifth of China's total CO_2 emissions. Several previous studies showed the potential of OCO-2 to detect and quantify strong point sources, but those studies were demonstrations rather than systematic analyses of OCO-2's ability to quantify regional emissions as presented here. The study by Zheng et al. is thus an important step forward. The applied methods are thorough and convincing. I particularly appreciated the conservative and careful selection of cases, for which emission quantification was safely possible. The results of the study nicely demonstrate the potential but also the great challenges offered by spaceborne CO_2 observations for emission quantification.

Emissions were estimated in the same way as in previous studies, i.e. by computing the integral amount of CO_2 in cross-sections through the plume multiplied by the wind component perpendicular to these cross-sections. However, there are novel elements that go beyond previous studies, notably the combination of a detailed emission inventory for China with a Gaussian plume approach where sources (e.g. cities) are not treated as individual plumes but as superpositions of multiple plumes emanating from individual area and point sources. Although the information from these super-positioned plumes was not used directly for plume quantification, it was used to attribute the plumes to specific emission sources, which was a critical step in the selection of suitable cases.

Overall, the paper is very well written and an important contribution to the growing literature on the quantitative interpretation of OCO-2 observations. I thus support publication after addressing the following points.

Response:

We thank the referee for the constructive and positive comments on our paper. We provide point-by-point responses as follows.

Main points:

- The title of the manuscript suggests that the study is about emissions of cities. However, the 60 plumes are not only from cities but also from "industrial regions". The authors should state explicitly how many of these plumes were representing emissions from cities, power plants and industrial complexes. This is important information for the planning of future satellite missions, since it is still not clear how well plumes from cities can be observed in comparison to those from power plants.

Response:

Among the 60 plumes that we analyzed, 33 plumes are from cities and the other 27 ones are from industrial regions. We now clarify this in the Sect. 3.1 as follow.

"The finally selected 60 cases include both densely populated urban areas (33 cases) and small industrial areas (27 cases) that gather many industrial plants."

We also revise the title of our paper to "Observing carbon dioxide emissions over China's cities and industrial areas with the Orbiting Carbon Observatory-2".

- The choice of a maximum distance of 50 km (page 4, line 100) between sources and OCO-2 track seems rather arbitrary. How does this choice affect the results? 50 km seems a rather short distance. More distant sources could contribute to the plumes and bias the corresponding estimates. The model-based study of Kuhlmann et al. (https://doi.org/10.5194/amt-12-6695-2019), for example, demonstrated that the plume of a power plant (Jänschwalde) 100 km away from a city (Berlin) could significantly overlap with the city plume in some cases.

Response:

Due to the steady-state assumption, the Gaussian plume model that was used to relate OCO-2 XCO_2 enhancements with emission sources is not reliable for long-range atmospheric transport (> 50 km, US EPA, 2015). We therefore prefer to restrict our analysis to the enhancements that can be related to sources within 50 km, thereby avoiding plumes originating from further away. For the cases that we selected, the agreement with the MEIC inventory (Fig. 3) suggests that we do not need to account for large emission sources outside the 50 km radius to interpret the enhancement.

- According to Bieser et al. (https://doi.org/10.1016/j.envpol.2011.04.030), roughly 90% of emissions from power plants occur between 200 m and 500 m above surface. How would emission estimates for power plants change using an average wind speed over this range rather than an average over 0–500 m (page 6, line 176)? Note that at the small distances between source and OCO-2 track considered in this study one cannot expect a homogeneous mixing of the plume over the depth of the PBL.

Response:

The 60 plumes that we analyzed are all from cities and industrial regions that have emission sources with various stack heights. The small industrial boilers and kilns, the major sources of CO_2 emissions in China, typically have smokestacks that are several tens of meters high. Therefore we used an average wind over 0–500 m to estimate the cross-sectional CO_2 fluxes from cities and industrial regions, which is the same configuration as Beirle et al. (2011) who also estimated city emissions (of nitrogen oxide) based on satellite observations.

Minor points and grammar:

- Page 1, line 18: Change "from the detailed China’s emission inventory" to "from China’s detailed emission inventory"

Response:

Corrected.

- P2, L34: "with the footprints" –> "with footprints"

Response:

Corrected.

- P2, L35: "natural CO_2 budget" -> "natural CO_2 budgets"

Response:

Corrected.

- P2, L36: "has allowed the initial insight" -> "has provided initial insight"

Response:

Corrected.

- P2, L46: "spaceborne CO_2 observation" -> "spaceborne CO_2 observations"

Response:

Corrected.

- P3, L64: "relies on the information about the wind" -> "relies on auxiliary information about winds"

Response:

Corrected.

- P3, L66: "provides the location" -> "provides the locations"

Response:

Corrected.

- P3, L75: "satellite sampling of OCO-2 capability" -> "sampling capability of OCO-2"

Response:

Corrected.

- P3, L77: "centered at the locations" -> "centered on the locations"

Response:

Corrected.

- P3, L86: Why should several XCO_2 anomalies belong to the same CO_2 plume? There is only a single transect per plume. Because of the moving windows?

Response:

The XCO_2 anomalies are those exceeding two sigmas of the spatial variability above the local average in each moving window. If a CO_2 plume crosses an OCO-2 track, the OCO-2 should observe a plume transect with XCO_2 enhancement, where there could be several XCO_2 anomalies larger than two sigmas above the local mean, although they correspond to the same CO_2 plume.

- P4, L91: "8 footprints if no is missing" -> "8 footprints if none is missing"

Response:

Corrected.

- P4, L93: "within CO_2 plume" -> "within the plume"

Response:

Corrected.

- P4, L104: Only a detail: Why is the along-wind distance measured in kilometres, but the across-wind distance in meters?

Response:

Here z (along-wind distance) has to be specified in kilometers to give $a \cdot z^{0.894}$ in meters (Bovensmann et al., 2010).

- P5, L136: I think it would be clearer to state "We find 49,322 cases with local XCO_2 enhancements". It wasn't clear to me initially whether these were individual pixels or plumes.

Response:

Corrected.

- P5, L144: 50 km is not an appropriate scale for synoptic transport. I suggest to simplify to ".. or transport of CO_2 over a longer distance"

Response:

Corrected.

- P5, L148: "in space to make it difficult" -> "in space making it difficult"

Response:

Corrected.

- P6, L153: It would be better to write "Although the total number of selected cases is small, it is several times larger .."

Response:

Corrected.

- P6, L163: "at about local 13:30" -> "at about 13:30 local time"

Response:

Corrected.

- P6, L164: "part of OCO-2 ground track" -> "part of the OCO-2 ground track"

Response:

Corrected.

- P6, L175: "CO_2 fluxes" -> "CO_2 flux"

Response:

Corrected.

- P6, L178: Why shifted by 1°? Maybe it would be clearer to state "shifted by 1° in this case".

Response:

Corrected.

- P7, L186: How was the uncertainty of the hourly emission rate of Qinhuangdao determined? Does the MEIC inventory include uncertainties?

Response:

Yes, the MEIC inventory includes uncertainties of city emission estimates (Zheng et al., 2018).

- P7, L194: There were 4 cases where the same source was quantified twice. It would be good to know how consistent those double quantifications are with the estimated uncertainty of <24%.

Response:

The emissions from 3 cities were quantified twice over the same season (i.e., cold or warm) at the same or different years. The consistency in these estimates for the same city, defined as the difference between one estimate and the two independent estimates mean, is 15–24%.

- P7, L203ff: The interpretation of the small differences of 5-6% between satellite based estimates and MEIC in different seasons is pushed too far in this section considering the uncertainties. At least the arguments should be presented as possible explanations rather than as facts (e.g. write "could be due to" rather than "are due to"). The over-interpretation of the results culminates in the statement that human respiration accounts for 38% of the (5.5%) difference and that the remaining difference could be due to a bias in MEIC. The numbers deduced from the satellite observations are not sufficiently robust to speculate about a bias in the inventory as small as 3 percent. Uncertainties in the method (notably the assumption that the 0-500 m average wind speed is representative) could easily explain such differences, probably also differences in the results between summer and winter since vertical mixing is different in these seasons.

Response:

We rewrote this paragraph as follows according to the reviewer's suggestion.

"The differences in the results between cold and warm seasons could be due to uncertainties in the emission estimate methods of both our OCO-2 based inversion and the MEIC inventory. The satellite-based larger estimates in the cold season could be partially due to the fact that human respiration contributes to urban CO_2 fluxes while not included in the MEIC inventory of fossil fuel and cement emissions. We make a rough estimate of the metabolic CO_2 release by multiplying an emission factor of 0.52 t-CO_2 yr^{-1} $person^{-1}$ (Prairie and Duarte, 2007) by the population living in each emitting area. The results suggest that human metabolic CO_2 emissions explain 8% of the larger satellite-based emission estimates on average in the cold season. The remaining difference could be due to the assumption that the 0-500 m average wind speed is representative of the transport wind in the plume diffusion, the natural processes like plant respiration, or the slight growth of fossil fuel emissions since 2013, but could also reflect some bias in the MEIC estimates. In the warm season, despite human respiration emissions, the satellite-based inversions give lower emission estimates possibly due to the carbon uptake by plants damping the XCO_2 enhancements (Mitchell et al., 2018), which makes anthropogenic emission signals not easily separated from the background in the satellite-based inversions."

- P8, L233: "principle, not all" -> "principle, but not all"

Response:

Corrected.

- P8, L235: "densely urban areas" -> "densely populated urban areas"

Response:

Corrected.

- P8, L44: The last section should be renamed to "Conclusions".

Response:

Corrected.

- P9, L271: "with less CO_2 inventory infrastructures" -> "with less advanced CO_2 inventory infrastructures"

Response:

Corrected.

- Figure 1: The blue bar should be called "XCO_2 anomalies" rather than "XCO_2 outliers"

Response:

Corrected.

References

Beirle, S., Boersma, K. F., Platt, U., Lawrence, M. G., and Wagner, T.: Megacity Emissions and Lifetimes of Nitrogen Oxides Probed from Space, Science, 333, 1737-1739, doi: 10.1126/science.1207824, 2011.

Bovensmann, H., Buchwitz, M., Burrows, J. P., Reuter, M., Krings, T., Gerilowski, K., Schneising, O., Heymann, J., Tretner, A., and Erzinger, J.: A remote sensing technique for global monitoring of power plant CO_2 emissions from space and related applications, Atmos. Meas. Tech., 3, 781-811, doi: 10.5194/amt-3-781-2010, 2010.

US EPA: Revision to the Guideline on Air Quality Models: Enhancements to the AERMOD Dispersion Modeling System and Incorporation of Approaches to Address Ozone and Fine Particulate Matter. Tech. rep. US Environmental Protection Agency #2060-AS54. https://www3.epa.gov/ttn/scram/11thmodconf/9930-11-OAR_AppendixW_Proposal.pdf, 2015.

Zheng, B., Zhang, Q., Davis, S. J., Ciais, P., Hong, C., Li, M., Liu, F., Tong, D., Li, H., and He, K.: Infrastructure Shapes Differences in the Carbon Intensities of Chinese Cities, Environ. Sci. Technol., doi: 10.1021/acs.est.7b05654, 2018.

Observing carbon dioxide emissions over China's cities and industrial areas with the Orbiting Carbon Observatory-2

Bo Zheng[1], Frederic Chevallier[1], Philippe Ciais[1], Gregoire Broquet[1], Yilong Wang[1, 2], Jinghui Lian[1], and Yuanhong Zhao[1]

[1]Laboratoire des Sciences du Climat et de l'Environnement, CEA-CNRS-UVSQ, UMR8212, Gif-sur-Yvette, France
[2]The Key Laboratory of Land Surface Pattern and Simulation, Institute of Geographical Sciences and Natural Resources Research, Chinese Academy of Sciences, Beijing, China

Correspondence to: Bo Zheng (bo.zheng@lsce.ipsl.fr)

Abstract. In order to track progress towards the global climate targets, the parties that signed the Paris Climate Agreement will regularly report their anthropogenic carbon dioxide (CO_2) emissions based on energy statistics and CO_2 emission factors. Independent evaluation of this self-reporting system is a fast-growing research topic. Here, we study the value of satellite observations of the column CO_2 concentrations to estimate CO_2 anthropogenic emissions with five years of the Orbiting Carbon Observatory-2 (OCO-2) retrievals over and around China. With the detailed information of emission source locations and the local wind, we successfully observe CO_2 plumes from ~~60~~ 46 cities and industrial regions over China and quantify their CO_2 emissions from the OCO-2 observations, which add up to a total of 1.~~3~~6 Gt CO_2 yr^{-1} that account for ~~17~~13% of mainland China's annual emissions. The number of cities whose emissions are constrained by OCO-2 here is three to ten times larger than previous studies that only focused on large cities and power plants in different locations around the world. Our satellite-based emission estimates are broadly consistent with the independent values from ~~the detailed~~ China's detailed emission inventory MEIC, but are more different from those of two widely used global gridded emission datasets (i.e., EDGAR and ODIAC), especially for the emission estimates for the individual cities. These results demonstrate some skill in the satellite-based emission quantification for isolated source clusters with the OCO-2, despite the sparse sampling of this instrument not designed for this purpose. This skill can be improved by future satellite missions that will have a denser spatial sampling of surface emitting areas, which will come soon in the early 2020s.

1 Introduction

The Paris Agreement on climate change requires all parties (countries) to report their anthropogenic greenhouse gas emissions and removals at least every two years within an enhanced transparency framework (UNFCCC, 2018). Then, starting in 2023, the country reports will periodically form the basis for a global stocktake that will assess collective progress in bringing the global greenhouse gas emissions consistent with global warming well below 2°C above pre-industrial levels. In order to address potential biases in this self-reporting mechanism, the contribution of independent observation systems is being increasingly

sought (IPCC, 2019). Our focus here is on the direct observation of fossil fuel carbon dioxide (CO_2) emission plumes from space and on the quantification of CO_2 emissions from this observation independently.

NASA's second Orbiting Carbon Observatory (OCO-2) polar satellite (Eldering et al., 2017) is one of the best existing instruments for the retrieval of column-averaged dry-air mole fraction of CO_2 (XCO_2). It observes the clear-sky and sun-lit part of the Earth with ~~the~~ footprints of a few km^2 (1.29 km × 2.25 km) gathered in a ~10 km wide swath for each orbit, particularly suitable for informing natural CO_2 budgets at the continental scales. It has already acquired more than five years of science data since its launch in July 2014, which has provided~~allowed the~~ initial insight into carbon fluxes from the tropical terrestrial ecosystems (Liu et al., 2017; Palmer et al., 2019) but not without ambivalence due to likely significant residual systematic errors in the OCO-2 XCO_2 retrievals (Chevallier, 2018).

Extending the use of OCO-2 to monitor fossil fuel CO_2 emissions is rather challenging because the excess XCO_2 generated by large cities or power plants typically reaches ~ 1% at best (Kort et al., 2012), which is about 4 ppm compared with an instrument noise typically around ~~1~~ 0.3–0.6 ppm (Worden et al., 2017) for a single sounding. This non-negligible noise in the XCO_2 retrievals is hardly balanced by the amount of data sampled near emission sources with a narrow swath, which hampers the detection of emission plumes and the precision of emission quantification. Only under rare occasions, the OCO-2 tracks cross CO_2 plumes downwind large cities (Labzovskii et al., 2019; Reuter et al., 2019) or power plants (Schwandner et al., 2017; Nassar et al., 2017; Zheng et al., 2019), limiting the possibility to quantify the corresponding CO_2 emissions to few cases within a year. So far, studies on the potential of spaceborne CO_2 observations to infer CO_2 emissions from large cities or power plants have relied on ~~the~~ Observing System Simulation Experiments (OSSEs) (Bovensmann et al., 2010; O'Brien et al., 2016; Broquet et al., 2018; Kuhlmann et al., 2019; Wang et al., 2020) and on several well-chosen cases with real OCO-2 retrievals (Nassar et al., 2017; Reuter et al., 2019; Zheng et al., 2019; Wu et al., 2020). To our knowledge, no attempt has been made yet to infer anthropogenic emissions from actual ~~satellite~~ OCO-2 data over a large area or a long period to evaluate a large-scale CO_2 budget.

Here we analyze all OCO-2 ground tracks between September 2014 and August 2019 over and around China, which is the largest emitter country in the world, in order to quantify CO_2 anthropogenic emissions at a large spatial extent over China. We develop a novel, simple, and effective approach to identify the CO_2 plumes from isolated emission clusters, to relate them unambiguously to nearby human emission sources, and to estimate the CO_2 emission fluxes causing each plume. The five-year period allows nearly one-~~fifth~~ sixth of all the emissions from mainland China to be observed, although OCO-2 swaths have a low probability to cross the emission plume from a given city. The budget of CO_2 emissions aggregating all the sources inferred from the satellite is compared to different emission inventories compiled by multiplying fuel consumption statistics by emission factors. Such a comparison, for the first time covering a significant fraction of the emissions from a country, demonstrates the potential of independently evaluating the self-reporting emission inventories from space.

2 Data and Method

2.1 Data input

We use version 9r of the OCO-2 bias-corrected XCO_2 retrievals (Kiel et al., 2019). We use the good quality data (xco2_quality_flag equals 0) over both land and ocean, and associated retrieval uncertainty statistics. Our inversion framework relies on auxiliary~~the~~ information about ~~the~~ winds and about the spatial distribution of emission sources, which are jointly used to link the observed CO_2 plume section with upwind local emission sources. We choose the spatially explicit Multi-resolution Emission Inventory for China (MEIC) dataset (Zheng et al., 2018a, 2018b) that provides the locations of ~100,000 individual industrial point sources (82% of mainland China emissions) and 0.1°×0.1° area source emissions (18% of mainland China emissions) developed for the year 2013. Unlike other inventories used to map industrial emissions using spatial proxies, MEIC includes local reports from each power plant and industrial operator about their emissions and geographic locations. The ERA5 reanalysis data (C3S, 2017) provides us with a first guess for the local wind fields.

2.2 OCO-2 XCO_2 local enhancement

The key steps of our method are the identification of an XCO_2 local enhancement from the satellite data that can be attributed to a CO_2 plume from a large emission source, its separation from the surrounding background, and the establishment of a numerical link to the nearby upwind human emission sources. They are designed to account for the specificity of the ~~satellite~~ sampling capability of OCO-2 ~~capability~~ and for the XCO_2 retrieval errors.

First, we look for XCO_2 anomalies along the OCO-2 tracks, which exceed 2 sigmas of the spatial variability above the local average within 200-km wide moving windows centered ~~at~~ on the locations of the anomalies. These anomalies potentially belong to significant CO_2 plumes. In each window corresponding to such an anomaly and with more than 200 high-quality retrievals (with ~800 retrievals if none are missing due to cloud contaminations or other issues in the retrieval algorithm), the following curve fitting is applied to the XCO_2 retrieval data along the OCO-2 track:

$$y = m \cdot x + b + \frac{A}{\sigma\sqrt{2\pi}} e^{\left[-(x-\mu)^2 / 2\sigma^2\right]} \quad (1)$$

where y is XCO_2 (ppm), x is the distance (km) along the OCO-2 track in a fitting window, m, b, A, μ, and σ are parameters that determine the curve shape, estimated by a nonlinear least-squares fit weighted by the reciprocal of XCO_2 uncertainty statistics. The linear part $m \cdot x + b$ represents the background level assuming the background is linear (Reuter et al., 2019), while the remaining part depicts a single XCO_2 peak with a Gaussian shape (Nassar et al., 2017). Several XCO_2 anomalies should belong to the same CO_2 plume: in order to only define a single equation for a given plume and the corresponding background, we fit the curve around each XCO_2 anomaly and select the one with the largest R^2. We also reject all cases with low R^2 (less than 0.25) to achieve better fitting performance.

Second, we select the cases when the range of $\mu \pm 3\sigma$ is fully covered by the 200-km window to achieve complete fitting curves that cover both the plume part and the wide range of local background. To make the curve fitting robust, we further select the

observational cases that have at least 3 valid cross-track footprints (8 footprints if none is missing) on average within the plume transect ($\mu \pm 2\sigma$) to constrain the shape of the fitted curve with enough data points. Finally, we check if the parameter A is positive and if the average XCO_2 value within the ~~CO_2-plumes~~ (defined as the average of raw XCO_2 retrievals within $\mu \pm 2\sigma$) minus the surrounding background concentration (derived as the average of raw XCO_2 retrievals outside 2σ) is larger than the standard deviation of the background values within 200 km. Only the cases that pass these two filtering criteria are finally identified as the XCO_2 local enhancements in this study.

2.3 Gaussian plume model

We use the Gaussian plume model (Bovensmann et al., 2010) to attribute the observed XCO_2 enhancement to a neighbor cluster of emission sources. We simulate the sum of XCO_2 plumes generated by each point source and each emission grid cell from the MEIC inventory within 50 km of the studied OCO-2 track with equations:

$$V = \sum_{\in 50km} \frac{F}{\sqrt{2\pi} \cdot a \cdot z^{0.894} \cdot u} e^{-\frac{1}{2}\left(\frac{n}{a \cdot z^{0.894}}\right)^2} \quad (2)$$

$$XCO_2 = V \cdot \frac{M_{air}}{M_{CO2}} \cdot \frac{g}{P_{surf} - w \cdot g} \cdot 1000 \quad (3)$$

where V is the CO_2 vertical column (g m^{-2}) downwind of the emission sources, F is the emission rate (g s^{-1}), u is the wind speed (m s^{-1}), z is the along-wind distance (km), n is the across-wind distance (m), and a is the atmospheric stability parameter. Equation (3) converts V (g m^{-2}) to XCO_2 (ppm), where M is the molecular weight (kg mol^{-1}), g is the gravitational acceleration (m s^{-2}), P_{surf} is the surface pressure (Pa), and w is the total column water vapor (kg m^{-2}).

F is derived from the MEIC emission inventory (Zheng et al., 2018b), including both point sources and 0.1°×0.1° area source emissions. Each grid cell of area sources is used as a point source in Equation (2). u is the average wind at 1000, 975, and 950 hPa to approximate the wind below 500 m (Beirle et al., 2011) at the time of the OCO-2 overpass, derived from the ERA5 reanalysis data (C3S, 2017). In the presence of relief, the average of the pressure-level winds is weighted towards the surface. a is a function of the atmospheric stability condition (Martin, 1976) determined by both the 10-m wind speed and the incoming solar radiation (Seinfeld and Pandis, 2006). Wind, solar radiation, and P_{surf} are all derived from the ERA5 reanalysis dataset (C3S, 2017), and w is adopted from the OCO-2 files.

2.4 Cross-sectional CO_2 flux estimate

We relate each satellite observed XCO_2 enhancement to anthropogenic emission sources within 50 km using the Gaussian plume model. We visually inspect the observed and modeled XCO_2 and further select the ones that exhibit a single and isolated CO_2 plume to attribute the plume to a neighbor cluster of emission sources and estimate the corresponding cross-sectional CO_2 fluxes. We remove the linear background from the fitted curve of Equation (1) and calculate the area under the remaining fitted curve to derive the CO_2 line density (ppm m), which can be converted to the unit of g m^{-1} through Equation (3). The errors in

the CO_2 line densities are those of the area under the fitted curve, mainly driven by the random errors of the XCO_2 retrievals and also by the Equation (1) that is not a perfect representation of actual CO_2 plumes. The standard error statistics for each parameter in Equation (1) are obtained from the weighted nonlinear least-squares fitting, which are propagated to calculate the uncertainties of the area under the fitted curve.

The CO_2 line densities are multiplied by the wind speed (m s^{-1}) in the direction normal to the OCO-2 tracks at the location of the plume peak to estimate cross-sectional CO_2 fluxes (g s^{-1}). The average wind below 500 m is used like in Equation (2). To reduce the errors in the wind direction, we allow rotation of the wind direction within 45° on each side of the ERA5 local wind direction to maximize the spatial correlation between the Gaussian plume-modeled and the OCO-2-observed XCO_2 according to Nassar et al. (2017). The derived cross-sectional CO_2 fluxes approximately represent upwind source emissions under steady-state atmospheric conditions, while changes in the atmospheric stability (e.g., strong turbulent diffusion) could make the cross-sectional flux diverge from the source emissions (Varon et al., 2018; Reuter et al., 2019).

3 Results

3.1 CO_2 emission plumes seen by satellite

The identification of CO_2 emission plumes crossed by the satellite field of view starts with the search for XCO_2 local enhancements. These are defined as XCO_2 peaks above the background along the thin OCO-2 tracks. As shown in Fig. 1, we have identified a total of 6,565 OCO-2 ground tracks over or around China between September 2014 and August 2019, with an even share between the cold-season (from September to February, 47%) and the warm-season ones (from March to August, 53%). We find 49,322 cases with local XCO_2 ~~local~~ enhancements that exceed 2 sigmas above the local average in a 200 km-wide moving window along the satellite tracks. However, 97% of these XCO_2 enhancements are removed after evaluation of the integrity of the plume section and of the spatial variation of surrounding background retrievals, leaving only 1,439 XCO_2 cases as potent candidates for retrieving emissions.

The second step consists in attempting to attribute the observed 1,439 CO_2 enhancements to nearby human emission sources. Only ~~355~~ 370 of the 1,439 XCO_2 local enhancements can be related to emission sources in the MEIC dataset using the Gaussian plume model within a 50-km upwind distance from each OCO-2 ground track. The other cases that reveal XCO_2 enhancement but no nearby emission sources within 50 km upwind are probably due to either OCO-2 XCO_2 retrieval errors at local scales, or sources missing in MEIC, or ~~synoptic~~ transport of CO_2~~,~~ over a ~~much~~ longer distance (Parazoo et al., 2011).

The third step is the quantification of cross-sectional CO_2 fluxes within the satellite observed CO_2 plumes. Only ~~64~~ 60 of the ~~355~~ 370 cases correspond to single isolated CO_2 plumes within a 200 km-wide window, which allow unambiguous attribution to an emission site or cluster. One reason why we reject the other ~~291~~ 310 cases is that they have two or more individual plumes. ~~(~~partially overlapping or separated~~), which are distant in space to making it difficult to merge into a single isolated emission plume transect~~. Some of the rejected cases also lack observation data of good quality (*xco2_quality_flag* equals 0) at a distance of several tens of kilometers due to significant retrieval errors in the local satellite observations.

The data filtering process retains more cold-season observations (6955%) than warm-season ones, in particular after the last first step (5652% cases are from the cold season after the second first step), due to favorable meteorological patterns during the cold season. Although Tthe total number of selected cases is small, it is several times larger than in previous studies that only focused on large cities and large power plants in different locations of the world (Nassar et al., 2017; Reuter et al., 2019; Wu et al., 2020). The finally selected 64 60 cases include both densely populated urban areas (33 cases) and small industrial areas (27 cases) that gather many industrial plants. The peak height of XCO_2 enhancement in the plumes ($A/(\sigma\sqrt{2\pi})$ in Equation (1)) is within 01.18–6.0 μmol mol^{-1} (abbreviated as ppm) above the average local background and 2–7 times higher than the standard deviation of background levels within 200 km. The width of observed CO_2 plumes, defined as the full width at half maximum of peak height, is estimated between 42.42 and 7461.72 km.

3.2 Quantifying CO_2 emissions: one city example

Figure 2 presents one example of the 64 60 selected cases. The emitter here is the city Qinhuangdao Anshan that has about one 1.5 million inhabitants. On October 17th 20182016, CO_2 emissions from Qinhuangdao Anshan were blown southward by a 17.61 m s^{-1} wind at the OCO-2 overpass time and generated an XCO_2 local enhancement offshore larger than 2 ppm (Fig. 2). At about local 13:30 local time, OCO-2 flew over the sea to the east of China (Fig. 2a), crossed the CO_2 plume transported from QinhuangdaoAnshan, and successfully observed the local enhancement near the northernmost southernmost part of the OCO-2 ground track (Fig. 2b).

We plot the XCO_2 retrieval data (grey dots in Fig. 2c) along the satellite ground track, the plot window of which is centered at the highest XCO_2 value in the CO_2 plume. We first fit the black curve (R^2 = 0.47) based on Equation (1) to depict the CO_2 plume transect. The local background is represented by a straight line $-32.63E-35 \cdot x + 404402.8 1$ that approximates a flat background of 4024.18 ppm. Then we subtract the background line from both the XCO_2 data and the fitted black curve to obtain the net enhancement of XCO_2 above the local background (pink dots and red curve in Fig. 2d). The maximum XCO_2 net enhancement (peak height of the red curve) is 2.7 4 ppm and the plume width is 1537.40 km. The CO_2 line density is estimated as 10.607 ± 0.041 t-CO_2 m^{-1} (central estimate ± 1σ) by computing the area under the red curve (the orange shade in Fig. 2d). The uncertainty is mainly caused by random errors of the single XCO_2 retrievals.

The CO_2 line density derived from the satellite retrievals is further multiplied by the wind speed in the normal direction to the OCO-2 track to quantify the cross-sectional CO_2 fluxes. We use the average wind below 500 m from the ERA5 reanalysis data. The ceiling height of 500 m is comparable to the maximum height that smoke plumes from power plants and industrial plants typically reach. The wind direction around AnshanQinhuangdao is optimized according to Nassar et al. (2017) and is shifted by 1° in this case to maximize the spatial correlation between the satellite-observed (Fig. 2d) and the model-simulated (Fig. 2e) XCO_2 enhancements. The wind speed in the normal direction to the OCO-2 track is then estimated as 02.6 m s^{-1} at the location of the maximum XCO_2 value (Fig. 2b). The CO_2 hourly flux at the satellite overpassing time is finally estimated as 35.74 ± 10.27 kt-CO_2 h^{-1}, considering uncertainties both in the CO_2 line density and in the wind speed.

The satellite observed CO_2 plume can be traced back to anthropogenic emission sources located in the urbanized area of the ~~Qinhuangdao~~ Anshan city by the Gaussian plume model combined with the local emission map given by the MEIC inventory. We use monthly, weekly, and diurnal emission time profiles by region and by source sector from MEIC to split the annual emission totals reported by MEIC to hourly emission rates during the satellite overpass. The MEIC hourly emission rate of ~~Qinhuangdao~~ Anshan is ~~6~~2.~~46~~ ± ~~1~~0.~~98~~ kt-CO_2 h^{-1}, which is close to the satellite-based inversion estimate.

3.3 CO_2 emission estimates for 60 ~~regions~~ cases in China

We quantify the CO_2 emissions corresponding to the ~~64~~ 60 CO_2 plumes selected from the five-year OCO-2 archive. These represent ~~60~~ 46 different urban areas or industrial regions in China. There are 14 regions whose emission plumes were observed twice in our selection of the satellite data. The ~~64~~ 60 CO_2 plumes present CO_2 line densities between 0.1 and 2.8 t-CO_2 m^{-1}, and hourly CO_2 fluxes at the time of the satellite overpass are estimated within the range of 0.3~~2~~–16~~5~~.0~~4~~ kt-CO_2 h^{-1} with the 1σ uncertainties of 20–~~28~~30%. The larger sources tend to present lower relative uncertainties, because a larger XCO_2 enhancement makes it easier to separate a plume from its background, and is thus more easily observed by the satellite. The inversions that estimate CO_2 emissions larger than 4 kt-CO_2 h^{-1} tend to constrain their relative uncertainties below ~~24~~25%.

We compare the satellite-based CO_2 hourly fluxes to the corresponding source emissions given by MEIC (Fig. 3), after applying emission time profiles to transform MEIC annual emissions into hourly emissions at the time of satellite overpass. Although the point source based MEIC emissions data is only for the year 2013, China's countrywide emissions remained stable between 2013 and 2017 and marginally grew only after 2017 (Friedlingstein et al., 2019). The satellite-based and MEIC estimated emissions are broadly consistent within a factor of two (solid dots in Fig. 3) with comparable uncertainties for the same individual estimates. ~~Both approaches estimate the same average CO_2 flux of the 64 emission plumes as 3.8 kt-CO_2 h^{-1}.~~ The average of satellite-based estimates is 27~~5~~.1~~5~~% higher than the MEIC values in the cold season (solid blue dots in Fig. 3), while 5~~6~~.0~~2~~% lower in the warm season (solid red dots in Fig. 3).

The differences in the results between cold and warm seasons could be due to uncertainties in the emission estimate methods of both our OCO-2 based inversion and the MEIC inventory. The satellite-based larger estimates in the cold season could be~~are~~ partially due to the fact that human respiration contributes to urban CO_2 fluxes while not included in the MEIC inventory of fossil fuel and cement emissions. We make a rough estimate of the metabolic CO_2 release by multiplying an emission factor of 0.52 t-CO_2 yr^{-1} $person^{-1}$ (Prairie and Duarte, 2007) by the population living in each emitting area. The results suggest that human metabolic CO_2 emissions explain ~~3~~8% of the larger satellite-based emission estimates on average in the cold season. The remaining difference could be due to the assumption that the 0–500 m average wind speed is representative of the transport wind in the plume diffusion, the natural processes like plant respiration, or ~~to~~ the slight growth of fossil fuel emissions since 2013, but could also reflect some bias in the MEIC estimates. In the warm season, despite human respiration emissions, the satellite-based inversions give lower emission estimates possibly due to the carbon uptake by plants ~~lower~~damping the XCO_2 enhancements ~~over a city~~ (Mitchell et al., 2018), which makes anthropogenic emission signals not easily ~~urban green spaces that are not~~ separated from the background ~~anthropogenic emissions~~ in the satellite-based inversion~~s method~~.

The uncertainties in the satellite-based emission estimates are driven by those of the local wind field and of the CO_2 line density derived from the XCO_2 retrievals. We reduce the errors in wind directions and consequently increase the R^2 of the linear correlation between satellite- and MEIC-based emission estimates across emitting areas from 0.~~16~~ 37 (open dots) to 0.5~~0~~7 (solid dots) as shown in Fig. 3. The magnitude of the wind speed uncertainty, typically considered 10–20% (Nassar et al., 2017; Varon et al., 2018; Reuter et al., 2019), is comparable to the uncertainty in the satellite-based CO_2 line densities (~~4~~3–~~19~~23% for the 6~~0~~4 emission plumes). In high wind-speed conditions, the CO_2 plumes are spread more quickly and thus cause smaller local enhancements, which weakens the signal of XCO_2 and causes larger uncertainties in the estimate of CO_2 line densities. Generally, our estimates reach lower relative uncertainties for larger emission cities under lower wind speeds.

3.4 Comparison with global bottom-up inventories

We extrapolate the satellite-based CO_2 hourly fluxes to annual total fluxes using emission time profiles, and compare them to two global bottom-up emission maps: ODIAC (Oda and Maksyutov, 2015, Oda et al., 2018) and EDGAR (Janssens-Maenhout et al., 2019). We use the cases between the years 2014 and 2018 when both inventories are available, and extract CO_2 emissions over each satellite-observed emitting area from the emission maps (Fig. 4). For the areas observed by the satellite in different years, we compute annual values from the corresponding inversions and average them for the comparison with ODIAC and EDGAR.

For individual estimates, ODIAC (Figs. 4b) and EDGAR (Figs. 4c) are broadly consistent with the annual budgets from the satellite-based inversions, but the fit is slightly better in the case of EDGAR. ~~For Beijing where MEIC remarkably agrees with the satellite estimate (Fig. 3), ODIAC and EDGAR estimate larger emissions by 322% and 202%, respectively. Such~~The large discrepancies are not surprising since global emission inventories typically involve large uncertainties at city scales (Gately and Hutyra, 2017; Gurney et al., 2019), because they disaggregate national emissions to gridded maps with simple proxies like population or nighttime light in the countries like China where they lack detailed direct local information. Only large power plants have exact geographic locations (from the CARMA global database (Wheeler and Ummel, 2008)), in principle, but not all of the industrial plants like MEIC. ~~The~~ ODIAC uses nightlights to disaggregate national emission estimates to grid cells, which may lead to an underestimation of road emissions in cities (Gately and Hutyra, 2017) and a misplacing of industrial emissions. ~~The~~ EDGAR relies on point source locations to allocate emissions in space while it still suffers from missing local information in China, and gridded population maps have to be used instead. Such an emission mapping approach overestimates emissions over densely populated cities in China (Zheng et al., 2017), because the industry plants, the primary CO_2 emission sources in China, are located far away from densely populated urban areas. The MEIC inventory estimates industrial emissions at the facility scale, transport emissions at the county scale, and residential emissions at the provincial scale, which can achieve better spatial accuracy in emissions estimates than the global emission inventories.

The sum of the emissions from the satellite-observed areas reaches 1.2~~58~~5 Gt CO_2 yr^{-1} (Fig. 4a), accounting for 1~~3~~7% of the mainland China's total emissions. The corresponding bottom-up estimates from ODIAC, EDGAR, and MEIC are 1.13~~39~~, 1.~~55~~38, and 1.~~52~~ 17 Gt CO_2 yr^{-1}, respectively. ODIAC emissions are ~~1~~9.6~~2~~% lower than the satellite-based estimates while

EDGAR emissions are ~~only 2~~10.4% ~~lower~~higher. The slight growth of the emissions from 2014 to 2018 (documented in, e.g., EDGAR) could alone explain mostly the ~~6~~4% lower value for MEIC (valid for the year 2013) than the satellite estimate. Overall, EDGAR matches the individual estimates from the satellite-based inversions better than ODIAC for the ~~17~~13% of mainland China's CO_2 emissions that are observed by the satellite. However, both of these two global emission inventories reveal large uncertainties in emission estimates for individual areas as shown in Figs. 4b and 4c.

4. ~~Discussion~~Conclusions

We developed a novel objective approach to quantify local anthropogenic CO_2 emissions from the OCO-2 XCO_2 satellite retrievals. The key of this method is a conservative selection of the satellite data that can be safely exploited for emission quantification. It also depends on the wind information and the information about the locations of human emission sources in the upwind vicinity of the selected OCO-2 tracks. Future developments could aim at refining the stringent data selection, or at improving the estimation of wind speed ~~estimation~~ or the description of the plume footprint, for instance using detailed regional atmospheric transport models but the current simplicity of our approach makes it easily applicable everywhere over the globe in principle. Our first regional analysis over mainland China suggests that ~~17~~13% of its CO_2 human emissions can be observed and constrained, to some extent, by five years of retrieval data from the OCO-2, a satellite instrument not designed for this task. The satellite-based emission inversion results are broadly consistent (R^2=0.50~~7~~, meaning we agree on broad classes of emitters) with the reliable point source-based MEIC regional inventory despite our simple modeling of the plume and of its background, and despite possible biases due to local non-fossil fuel emissions or local sinks that contribute to the plume intensity. We also use the satellite-based estimates as a rough independent evaluation of two global bottom-up inventories, ODIAC and EDGAR.

There is still a large gap between what the satellite can see and what the National Greenhouse Gas Inventory reports submitted to the United Nations Framework Convention on Climate Change (UNFCCC), mentioned at the start of the introduction. The former is made of specific emission plumes linked to recent emission events without any sectoral distinction within the plume. The latter is made of the country- and annual-scale emission values assigned to specific human-caused source/sink categories. The exhaustiveness of the MEIC inventory, which involved detailed analysis of the fine spatial and temporal emission patterns, allowed us to bridge most of this gap for a time period when Chinese emissions did not vary much, but few countries have such a detailed geospatial inventory of their emissions and are able to update it timely for such a task. We also acknowledge the limitations of the emission temporal profiles even from the detailed MEIC inventory. The sparse sampling of the OCO-2 instrument, despite the good precision of individual soundings, will partly be overcome by the next-generation of CO_2-dedicated imagery satellites, such as the CO_2 Monitoring mission (CO2M) in Europe (Clery, 2019; Janssens-Maenhout et al., 2020) and the Geostationary Carbon Cycle Observatory (GeoCarb) in the U.S. (Moore III et al., 2018) that will have denser spatial coverage. However, their measurement principle still relies on sunlight and will prevent us from well sampling the emission diurnal cycle. The need for a good knowledge of the emission space-time patterns (not only the emission values) will

therefore remain for the comparison between the national inventories and the satellite-based estimates. However, for countries with less advanced CO_2 inventory infrastructures (typically non-Annex I parties to UNFCCC), we could also envisage an incremental approach where both bottom-up and top-down estimates are developed together in parallel.

Data availability

The version 9r of the OCO-2 bias-corrected XCO_2 retrievals were downloaded from the data archive maintained at the NASA Goddard Earth Science Data and Information Services Center (https://oco2.gesdisc.eosdis.nasa.gov/data/s4pa/OCO2_DATA/OCO2_L2_Lite_FP.9r/, last access: 12 February 2020; Kiel et al., 2019). The ERA5 reanalysis data were acquired from the Copernicus Climate Change Service Climate Data Store (https://cds.climate.copernicus.eu/, last access: 12 February 2020; C3S, 2017).

Author contributions

BZ, FC, and PC designed the study. BZ processed the observational data and estimated the CO_2 fluxes from the satellite observations. BZ prepared the paper with contributions from all coauthors.

Competing interests

The authors declare that they have no conflict of interest.

Acknowledgements

The OCO-2 retrievals were produced by the OCO-2 project at the Jet Propulsion Laboratory, California Institute of Technology, and obtained from the OCO-2 data archive maintained at the NASA Goddard Earth Science Data and Information Services Center.

References

Beirle, S., Boersma, K. F., Platt, U., Lawrence, M. G., and Wagner, T.: Megacity Emissions and Lifetimes of Nitrogen Oxides Probed from Space, Science, 333, 1737-1739, doi: 10.1126/science.1207824, 2011.

Bovensmann, H., Buchwitz, M., Burrows, J. P., Reuter, M., Krings, T., Gerilowski, K., Schneising, O., Heymann, J., Tretner, A., and Erzinger, J.: A remote sensing technique for global monitoring of power plant CO_2 emissions from space and related applications, Atmos. Meas. Tech., 3, 781-811, doi: 10.5194/amt-3-781-2010, 2010.

Broquet, G., Bréon, F. M., Renault, E., Buchwitz, M., Reuter, M., Bovensmann, H., Chevallier, F., Wu, L., and Ciais, P.: The potential of satellite spectro-imagery for monitoring CO_2 emissions from large cities, Atmos. Meas. Tech., 11, 681-708, doi: 10.5194/amt-11-681-2018, 2018.

Chevallier, F.: Comment on "Contrasting carbon cycle responses of the tropical continents to the 2015–2016 El Niño", Science, 362, eaar5432, doi: 10.1126/science.aar5432, 2018.

Clery, D.: Space budget boost puts Europe in lead to monitor carbon from space, Science, 2019.

Copernicus Climate Change Service (C3S) (2017): ERA5: Fifth generation of ECMWF atmospheric reanalyses of the global climate, Copernicus Climate Change Service Climate Data Store (CDS), https://cds.climate.copernicus.eu/cdsapp#!/home (accessed in Aug 2019).

Eldering, A., Wennberg, P. O., Crisp, D., Schimel, D. S., Gunson, M. R., Chatterjee, A., Liu, J., Schwandner, F. M., Sun, Y., O'Dell, C. W., Frankenberg, C., Taylor, T., Fisher, B., Osterman, G. B., Wunch, D., Hakkarainen, J., Tamminen, J., and Weir, B.: The Orbiting Carbon Observatory-2 early science investigations of regional carbon dioxide fluxes, Science, 358, eaam5745, doi: 10.1126/science.aam5745, 2017.

Friedlingstein, P., Jones, M. W., O'Sullivan, M., Andrew, R. M., Hauck, J., Peters, G. P., Peters, W., Pongratz, J., Sitch, S., Le Quéré, C., Bakker, D. C. E., Canadell, J. G., Ciais, P., Jackson, R. B., Anthoni, P., Barbero, L., Bastos, A., Bastrikov, V., Becker, M., Bopp, L., Buitenhuis, E., Chandra, N., Chevallier, F., Chini, L. P., Currie, K. I., Feely, R. A., Gehlen, M., Gilfillan, D., Gkritzalis, T., Goll, D. S., Gruber, N., Gutekunst, S., Harris, I., Haverd, V., Houghton, R. A., Hurtt, G., Ilyina, T., Jain, A. K., Joetzjer, E., Kaplan, J. O., Kato, E., Klein Goldewijk, K., Korsbakken, J. I., Landschützer, P., Lauvset, S. K., Lefèvre, N., Lenton, A., Lienert, S., Lombardozzi, D., Marland, G., McGuire, P. C., Melton, J. R., Metzl, N., Munro, D. R., Nabel, J. E. M. S., Nakaoka, S. I., Neill, C., Omar, A. M., Ono, T., Peregon, A., Pierrot, D., Poulter, B., Rehder, G., Resplandy, L., Robertson, E., Rödenbeck, C., Séférian, R., Schwinger, J., Smith, N., Tans, P. P., Tian, H., Tilbrook, B., Tubiello, F. N., van der Werf, G. R., Wiltshire, A. J., and Zaehle, S.: Global Carbon Budget 2019, Earth Syst. Sci. Data, 11, 1783-1838, doi: 10.5194/essd-11-1783-2019, 2019.

Gately, C. K., and Hutyra, L. R.: Large Uncertainties in Urban-Scale Carbon Emissions, J. Geophys. Res. Atmos., 122, 11,242-211,260, doi: 10.1002/2017jd027359, 2017.

Gurney, K. R., Liang, J., O'Keeffe, D., Patarasuk, R., Hutchins, M., Huang, J., Rao, P., and Song, Y.: Comparison of Global Downscaled Versus Bottom-Up Fossil Fuel CO_2 Emissions at the Urban Scale in Four U.S. Urban Areas, J. Geophys. Res. Atmos., 124, 2823-2840, doi: 10.1029/2018jd028859, 2019.

IPCC (Intergovernmental Panel on Climate Change): 2019 Refinement to the 2006 IPCC Guidelines for National Greenhouse Gas Inventories, https://www.ipcc-nggip.iges.or.jp/public/2019rf/, 2019.

Janssens-Maenhout, G., Crippa, M., Guizzardi, D., Muntean, M., Schaaf, E., Dentener, F., Bergamaschi, P., Pagliari, V., Olivier, J. G. J., Peters, J. A. H. W., van Aardenne, J. A., Monni, S., Doering, U., Petrescu, A. M. R., Solazzo, E., and Oreggioni, G. D.: EDGAR v4.3.2 Global Atlas of the three major greenhouse gas emissions for the period 1970–2012, Earth Syst. Sci. Data, 11, 959-1002, doi: 10.5194/essd-11-959-2019, 2019.

Janssens-Maenhout, G., Pinty, B., Dowell, M., Zunker, H., Andersson, E., Balsamo, G., Bézy, J.-L., Brunhes, T., Bösch, H., Bojkov, B., Brunner, D., Buchwitz, M., Crisp, D., Ciais, P., Counet, P., Dee, D., Denier van der Gon, H., Dolman, H., Drinkwater, M., Dubovik, O., Engelen, R., Fehr, T., Fernandez, V., Heimann, M., Holmlund, K., Houweling, S., Husband, R., Juvyns, O., Kentarchos, A., Landgraf, J., Lang, R., Löscher, A., Marshall, J., Meijer, Y., Nakajima, M., Palmer, P. I., Peylin, P., Rayner, P., Scholze, M., Sierk, B., Tamminen, J., and Veefkind, P.: Towards an operational anthropogenic CO_2 emissions monitoring and verification support capacity, Bulletin of the American Meteorological Society, doi: 10.1175/bams-d-19-0017.1, 2020.

Kiel, M., O'Dell, C. W., Fisher, B., Eldering, A., Nassar, R., MacDonald, C. G., and Wennberg, P. O.: How bias correction goes wrong: measurement of XCO_2 affected by erroneous surface pressure estimates, Atmos. Meas. Tech., 12, 2241-2259, doi: 10.5194/amt-12-2241-2019, 2019.

Kort, E. A., Frankenberg, C., Miller, C. E., and Oda, T.: Space-based observations of megacity carbon dioxide, Geophys. Res. Lett., 39, doi: 10.1029/2012gl052738, 2012.

Kuhlmann, G., Broquet, G., Marshall, J., Clément, V., Löscher, A., Meijer, Y., and Brunner, D.: Detectability of CO_2 emission plumes of cities and power plants with the Copernicus Anthropogenic CO_2 Monitoring (CO2M) mission, Atmos. Meas. Tech., 12, 6695-6719, doi: 10.5194/amt-12-6695-2019, 2019.

Labzovskii, L. D., Jeong, S.-J., and Parazoo, N. C.: Working towards confident spaceborne monitoring of carbon emissions from cities using Orbiting Carbon Observatory-2, Remote Sensing of Environment, 233, 111359, doi: 10.1016/j.rse.2019.111359, 2019.

Liu, J., Bowman, K. W., Schimel, D. S., Parazoo, N. C., Jiang, Z., Lee, M., Bloom, A. A., Wunch, D., Frankenberg, C., Sun, Y., O'Dell, C. W., Gurney, K. R., Menemenlis, D., Gierach, M., Crisp, D., and Eldering, A.: Contrasting carbon cycle responses of the tropical continents to the 2015–2016 El Niño, Science, 358, eaam5690, doi: 10.1126/science.aam5690, 2017.

Martin, D. O.: Comment On"The Change of Concentration Standard Deviations with Distance", Journal of the Air Pollution Control Association, 26, 145-147, doi: 10.1080/00022470.1976.10470238, 1976.

Mitchell, L. E., Lin, J. C., Bowling, D. R., Pataki, D. E., Strong, C., Schauer, A. J., Bares, R., Bush, S. E., Stephens, B. B., Mendoza, D., Mallia, D., Holland, L., Gurney, K. R., and Ehleringer, J. R.: Long-term urban carbon dioxide observations reveal spatial and temporal dynamics related to urban characteristics and growth, Proc. Natl. Acad. Sci., 115, 2912-2917, doi: 10.1073/pnas.1702393115, 2018.

Moore III, B., Crowell, S. M. R., Rayner, P. J., Kumer, J., O'Dell, C. W., O'Brien, D., Utembe, S., Polonsky, I., Schimel, D., and Lemen, J.: The Potential of the Geostationary Carbon Cycle Observatory (GeoCarb) to Provide Multi-scale Constraints on the Carbon Cycle in the Americas, Frontiers in Environmental Science, 6, doi: 10.3389/fenvs.2018.00109, 2018.

Nassar, R., Hill, T. G., McLinden, C. A., Wunch, D., Jones, D. B. A., and Crisp, D.: Quantifying CO_2 Emissions From Individual Power Plants From Space, Geophys. Res. Lett., 44, 10,045-010,053, doi: 10.1002/2017gl074702, 2017.

O'Brien, D. M., Polonsky, I. N., Utembe, S. R., and Rayner, P. J.: Potential of a geostationary geoCARB mission to estimate surface emissions of CO_2, CH_4 and CO in a polluted urban environment: case study Shanghai, Atmos. Meas. Tech., 9, 4633-4654, doi: 10.5194/amt-9-4633-2016, 2016.

Oda, T., and Maksyutov, S.: ODIAC Fossil Fuel CO_2 Emissions Dataset (ODIAC2019), Center for Global Environmental Research, National Institute for Environmental Studies, doi:10.17595/20170411.001, 2015. (accessed on 2019/12/20)

Oda, T., Maksyutov, S., and Andres, R. J.: The Open-source Data Inventory for Anthropogenic CO_2, version 2016 (ODIAC2016): a global monthly fossil fuel CO_2 gridded emissions data product for tracer transport simulations and surface flux inversions, Earth Syst. Sci. Data, 10, 87-107, doi: 10.5194/essd-10-87-2018, 2018.

Palmer, P. I., Feng, L., Baker, D., Chevallier, F., Bösch, H., and Somkuti, P.: Net carbon emissions from African biosphere dominate pan-tropical atmospheric CO_2 signal, Nature Communications, 10, 3344, doi: 10.1038/s41467-019-11097-w, 2019.

Parazoo, N. C., Denning, A. S., Berry, J. A., Wolf, A., Randall, D. A., Kawa, S. R., Pauluis, O., and Doney, S. C.: Moist synoptic transport of CO_2 along the mid-latitude storm track, Geophys. Res. Lett., 38, doi: 10.1029/2011gl047238, 2011.

Prairie, Y. T., and Duarte, C. M.: Direct and indirect metabolic CO_2 release by humanity, Biogeosciences, 4, 215-217, doi: 10.5194/bg-4-215-2007, 2007.

Reuter, M., Buchwitz, M., Schneising, O., Krautwurst, S., O'Dell, C. W., Richter, A., Bovensmann, H., and Burrows, J. P.: Towards monitoring localized CO_2 emissions from space: co-located regional CO_2 and NO_2 enhancements observed by the OCO-2 and S5P satellites, Atmos. Chem. Phys., 19, 9371-9383, doi: 10.5194/acp-19-9371-2019, 2019.

Seinfeld, J. H., and Pandis, S. N.: Atmospheric chemistry and physics: from air pollution to climate change, John Wiley & Sons, Inc., Hoboken, p. 750, 2006.

Schwandner, F. M., Gunson, M. R., Miller, C. E., Carn, S. A., Eldering, A., Krings, T., Verhulst, K. R., Schimel, D. S., Nguyen, H. M., Crisp, D., O'Dell, C. W., Osterman, G. B., Iraci, L. T., and Podolske, J. R.: Spaceborne detection of localized carbon dioxide sources, Science, 358, eaam5782, doi: 10.1126/science.aam5782, 2017.

Varon, D. J., Jacob, D. J., McKeever, J., Jervis, D., Durak, B. O. A., Xia, Y., and Huang, Y.: Quantifying methane point sources from fine-scale satellite observations of atmospheric methane plumes, Atmos. Meas. Tech., 11, 5673-5686, doi: 10.5194/amt-11-5673-2018, 2018.

Wang, Y., Broquet, G., Bréon, F. M., Lespinas, F., Buchwitz, M., Reuter, M., Meijer, Y., Loescher, A., Janssens-Maenhout, G., Zheng, B., and Ciais, P.: PMIF v1.0: an inversion system to estimate the potential of satellite observations to monitor fossil fuel CO_2 emissions over the globe, Geosci. Model Dev. Discuss., 2020, 1-27, doi: 10.5194/gmd-2019-326, 2020.

Wheeler, D., and Ummel, K.: Calculating Carma: Global Estimation of CO_2 Emissions from the Power Sector, Available at SSRN: https://ssrn.com/abstract=1138690 or http://dx.doi.org/10.2139/ssrn.1138690, 2008.

Worden, J. R., Doran, G., Kulawik, S., Eldering, A., Crisp, D., Frankenberg, C., O'Dell, C., and Bowman, K.: Evaluation and attribution of OCO-2 XCO_2 uncertainties, Atmos. Meas. Tech., 10, 2759-2771, doi: 10.5194/amt-10-2759-2017, 2017.

Wu, D., Lin, J., Oda, T., and Kort, E.: Space-based quantification of per capita CO_2 emissions from cities, Environ. Res. Lett 2020.

UNFCCC (United Nation Framework Convention on Climate Change): Decision 18/CMA.1 Modalities, procedures and guidelines for the transparency framework for action and support referred to in Article 13 of the Paris Agreement, FCCC/PA/CMA/2018/Add.2, 2018.

Zheng, B., Zhang, Q., Tong, D., Chen, C., Hong, C., Li, M., Geng, G., Lei, Y., Huo, H., and He, K.: Resolution dependence of uncertainties in gridded emission inventories: a case study in Hebei, China, Atmos. Chem. Phys., 17, 921-933, doi: 10.5194/acp-17-921-2017, 2017.

Zheng, B., Tong, D., Li, M., Liu, F., Hong, C., Geng, G., Li, H., Li, X., Peng, L., Qi, J., Yan, L., Zhang, Y., Zhao, H., Zheng, Y., He, K., and Zhang, Q.: Trends in China's anthropogenic emissions since 2010 as the consequence of clean air actions, Atmos. Chem. Phys., 18, 14095-14111, doi: 10.5194/acp-18-14095-2018, 2018a.

Zheng, B., Zhang, Q., Davis, S. J., Ciais, P., Hong, C., Li, M., Liu, F., Tong, D., Li, H., and He, K.: Infrastructure Shapes Differences in the Carbon Intensities of Chinese Cities, Environ. Sci. Technol., doi: 10.1021/acs.est.7b05654, 2018b.

Zheng, T., Nassar, R., and Baxter, M.: Estimating power plant CO_2 emission using OCO-2 XCO_2 and high resolution WRF-Chem simulations, Environ. Res. Lett., 14, 085001, doi: 10.1088/1748-9326/ab25ae, 2019.

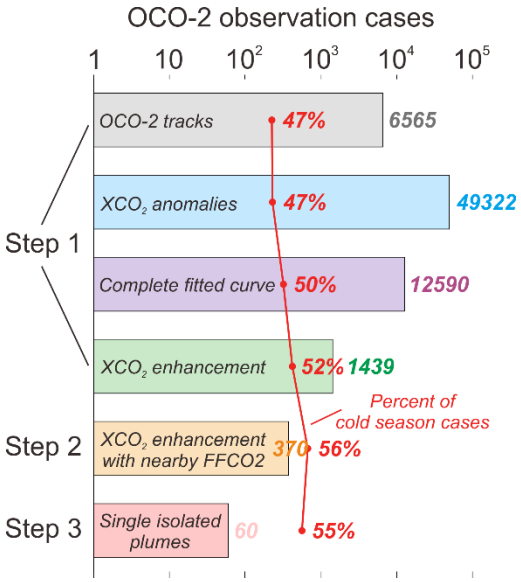

Figure 1: OCO-2 XCO_2 observation cases contained in each processing step. Step 1 starts from 6,565 OCO-2 tracks around and over China between September 2014 and August 2019 (grey bar) and finds 49,322 XCO_2 anomalies along the OCO-2 tracks (blue bar). 12,590 anomalies (purple bar) and their surrounding data points within a 200 km-wide window can be fitted by a complete nonlinear curve using Equation (1), of which 1,439 XCO_2 anomalies (green bar) are identified as local enhancement significantly higher than the background. Step 2 uses the Gaussian plume model to select 37055 XCO_2 enhancements (yellow bar) that can be traced back to upwind fossil fuel emission sources within 50 km. In step 3, we finally select the 604 cases with single isolated CO_2 plumes to quantify the CO_2 emissions. The red curve shows the percentage of cold-season observational cases in each bar. The detail of each step is described in Sect. 2.

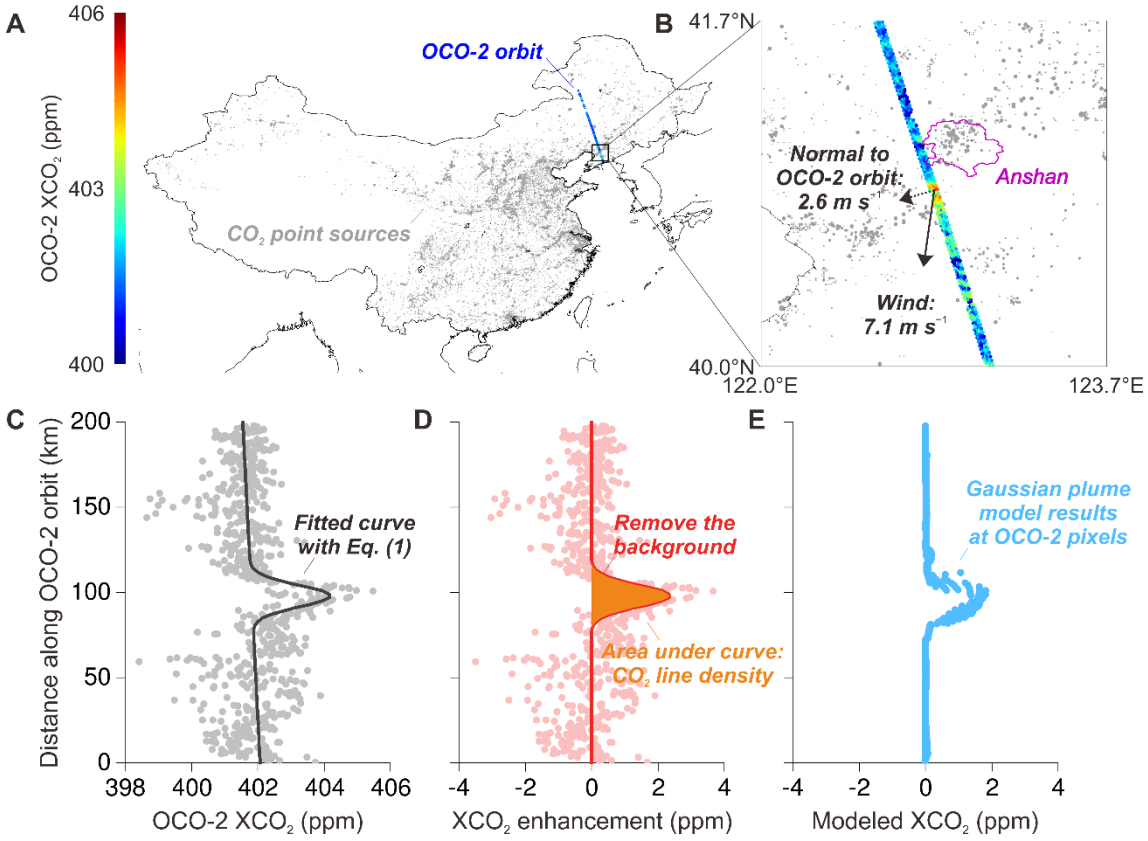

Figure 2: Quantification of CO_2 emissions from ~~Qinhuangdao~~Anshan. (A) The OCO-2 orbit on October 17th ~~2018~~ 2016 is plotted on the map of MEIC emission point sources. (B) Zoom in closer to see OCO-2 XCO_2 data, local wind speed, and wind direction. The width of the track is made of eight cross-track OCO-2 footprints. (C) The valid XCO_2 data points (grey dots) plotted along the OCO-2 orbit with a fitted curve (black) based on Equation (1). (D) The XCO_2 enhancement (red dots) above background, the fitted curve (red), and the area under the curve (orange shade). (E) The modeled XCO_2 enhancement (blue dots) by the Gaussian plume model combined with the MEIC emission inventory.

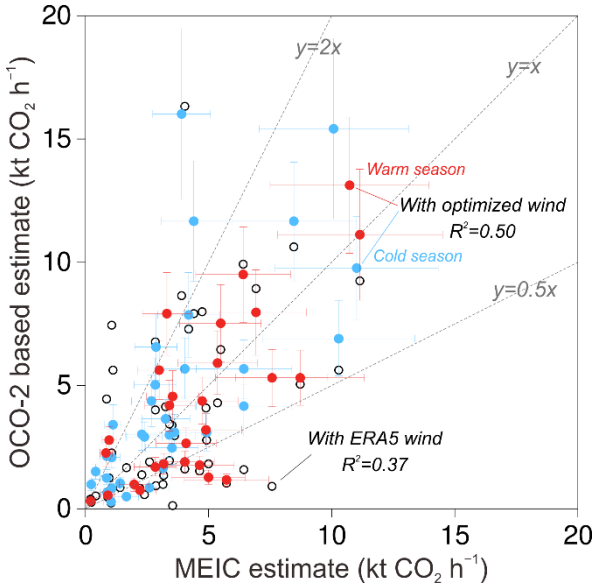

Figure 3: Comparison between OCO-2 based and MEIC estimated CO_2 hourly fluxes. Each dot represents one of the ~~64~~ 60 plume cases selected in this study, plotted according to the MEIC estimated CO_2 flux (x-axis) and the OCO-2-based estimate (y-axis). The open dots are OCO-2 estimates using the ERA5 wind data, while the solid dots use the optimized wind and distinguish the warm-season (red dots) and the cold-season (blue dots) cases.

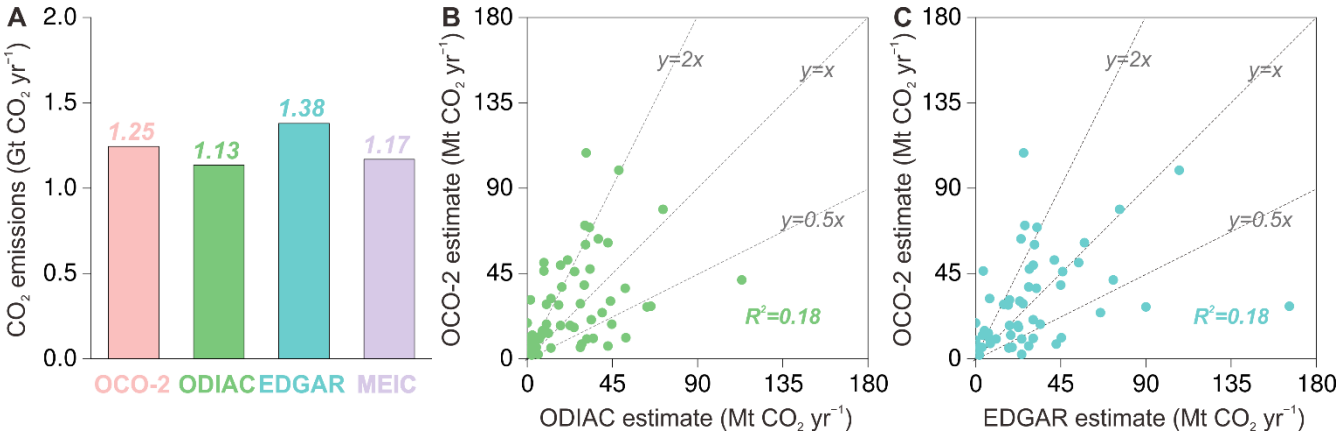

Figure 4: Comparing OCO-2 based CO_2 emission estimates with bottom-up inventories. (A) The sum of emissions from the ~~60~~ different regions observed by OCO-2 between the years 2014 and 2018, including OCO-2 estimates (scaled up to annual emissions based on MEIC emission time profiles, pink bar), ODIAC (green bar), EDGAR (blue bar), and MEIC (purple bar) estimates. (B) Comparison of regional CO_2 emissions between OCO-2-based (y-axis) and ODIAC estimates (x-axis). (C) Comparison of regional CO_2 emissions between OCO-2-based (y-axis) and EDGAR estimates (x-axis).